frontiers in Electronics

ORIGINAL RESEARCH
published: 23 April 2021
doi: 10.3389/felec.2021.643687

Improved Stability of Organic Photovotlaic Devices With $FeCl_3$ Intercalated Graphene Electrodes

Kieran K. Walsh[1,2], *Conor Murphy*[1,2], *Saverio Russo*[1] *and Monica F. Craciun*[1]*

[1] College of Engineering and Mathematical Sciences, University of Exeter, Exeter, United Kingdom, [2] XM2 Centre for Doctoral Training in Metamaterials, University of Exeter, Exeter, United Kingdom

In this paper, we present the first organic photovoltaic (OPV) devices fabricated with $FeCl_3$ intercalated few layer graphene (i-FLG) electrodes. i-FLG electrodes were first fabricated and characterized by electrical and spectroscopic means, showing enhanced conductive properties compared to pristine graphene. These electrodes were then used in the fabrication of OPV devices and tested against devices made with commercially available Indium Tin Oxide (ITO) electrodes. Both types of device achieved similar efficiencies, while the i-FLG based device exhibited superior charge transport properties due to the increase in work function characterizing i-FLG. Both types of device underwent a stability study using both periodic and continuous illumination measurements, which revealed i-FLG based OPVs to be significantly more stable than those based on ITO. These improvements are expected to translate to increased device lifetimes and a greater total energy payback from i-FLG based photovoltaic devices. These results highlight the potential benefits of using intercalated graphene materials as an alternative to ITO in photovoltaic devices.

Keywords: photovoltaics, organic, stability, graphene, electrode, intercalation, optoelectronics

Edited by:
Jiang Wu,
University of Electronic Science and Technology of China, China

Reviewed by:
Emmanuel Stratakis,
Foundation for Research and Technology Hellas, Greece
Yaoguang Rong,
Huazhong University of Science and Technology, China

***Correspondence:**
Monica F. Craciun
m.f.craciun@exeter.ac.uk

Specialty section:
This article was submitted to Optoelectronics, a section of the journal Frontiers in Electronics

Received: *18 December 2020*
Accepted: *11 March 2021*
Published: *23 April 2021*

Citation:
Walsh KK, Murphy C, Russo S and Craciun MF (2021) Improved Stability of Organic Photovotlaic Devices With $FeCl_3$ Intercalated Graphene Electrodes. Front. Electron. 2:643687. doi: 10.3389/felec.2021.643687

1. INTRODUCTION

Increasing concerns over the threat of climate change are driving requirements for a substantial change to our methods of energy production. Photovoltaic energy harvesting promises to provide a renewable source of energy with far less associated CO_2 emissions than conventional fossil fuels (Pehl et al., 2017), and has the potential to meet a greater energy need than all other renewable energy sources combined (Darling and You, 2013). Yet the high monetary and material cost of large scale manufacture and installation of solar cells has proved a barrier to many promising photovoltaic technologies in the past (Darling and You, 2013). For a new photovoltaic technology to rise through the energy market it must not only have a high efficiency, but also a long enough device lifetime to pay back the energy cost of fabrication. This is quantified by the Energy Payback Time (EPBT) metric, being the time required for a device to operate in order to repay the energy cost of the device's fabrication. Organic Photovoltaic (OPV) devices have significantly shorter EPBTs than conventional Si solar cells, on the order of days (Espinosa et al., 2012) as opposed to years for Si devices (Fthenakis and Kim, 2011; Bhandari et al., 2015; Malinowski et al., 2017). OPVs have the potential to provide a lower manufacturing cost than conventional photovoltaic technologies. However, one of the key contributions to the energy cost of fabrication for OPV devices is the cost required to produce the Indium Tin Oxide (ITO) electrode (Espinosa et al., 2011), accounting for up to 87% of the energy cost of fabrication for OPV devices. The replacement

of ITO in OPV devices has the potential to reduce production costs to the point where OPV technologies can provide cheaper energy than alternative Photovoltaic technologies (Darling and You, 2013). Another key requirement for an increased EPBT is the stability of OPV devices. Various degradation pathways present in the OVP devices have been identified, including the thermal stability of the active layers (Wong et al., 2014), photo-oxidation (Razzell-Hollis et al., 2014; Speller et al., 2019), atmospheric oxidation (Weu et al., 2019), and the ingress of water into the cell (Glen et al., 2016). Apart from these degradation pathways, there is significant evidence that ITO contributes to the degradation due to the ingress of indium ions into the active layers, caused by the acidic conditions from the PEDOT:PSS Hole Transport Layers (HTL) (Gallardo et al., 2007; Wu et al., 2007; Sharma et al., 2011). Finding a suitable electrode to replace ITO is therefore paramount to the development of OPV technologies and the lowered cost of renewable energy.

One such candidate for a replacement electrode is graphene. Gaining notoriety after its discovery in 2004 (Novoselov et al., 2004), graphene quickly became one of the most rigorously studied materials of the twenty-first century due to its impressive electronic (Novoselov et al., 2005; Castro Neto et al., 2009), mechanical (Lee et al., 2008), and optical properties (Nair et al., 2008). Due to its two dimensional (2D) hexagonal arrangement of carbon atoms, graphene has both excellent mechanical strength and conductivity, while also being thin enough to have excellent transmission to light in the visible range. These combined properties not only make graphene an excellent material for use as a transparent electrode across many applications, but are especially promising for OPV devices, as it allows the devices to utilize the OPV materials' inherent flexibility. However, the fabrication of a suitable graphene electrode that can compete with the properties of ITO has proved to be a challenge. Large area samples of graphene grown by Chemical Vapor Deposition (CVD) have a high sheet resistance when compared to mechanically exfoliated graphene (Sun et al., 2010), and a much higher sheet resistance than ITO. Likewise, graphene exfoliated in solution or solution processed reduced graphene oxide has also shown promise for large area optoelectronic device applications due to its low cost method of production, further reducing the EPBT required of the device. Though this has been the subject of much research (Kymakis et al., 2013; Balis et al., 2016) the sheet resistance of these samples remains many orders of magnitude higher than that of ITO (Kymakis et al., 2011), making it difficult to achieve comparable efficiencies with such electrodes. However, the sheet resistance of graphene can be significantly reduced through doping, either by chemical or physical means (Brunetti et al., 2015; Shin et al., 2018). Out of the many explored routes to improve graphene's conductive properties, few methods have shown more promise than intercalation of Few Layer Graphene (FLG) by $FeCl_3$ (Khrapach et al., 2012; Bointon et al., 2014). In this process, $FeCl_3$ molecules are able to penetrate between the layers in the graphene, causing a strong p-doping effect. This results in a reduction of the sheet resistance of the intercalated Few Layer graphene (i-FLG) by up to two orders of magnitude (Khrapach et al., 2012), as well as a significant increase in the sample's Work Function (WF) (Bointon et al., 2015). In addition to these highly desirable traits, the i-FLG is stable to high levels of humidity across a wide range of temperatures (Wehenkel et al., 2015) and can be processed in large areas (Bointon et al., 2015; Walsh et al., 2018). i-FLG has so far been demonstrated as a transparent electrode in optoelectronic devices such as photodetectors (Withers et al., 2013; de Sanctis et al., 2017) and flexible lighting devices (Torres Alonso et al., 2016).

In this investigation we fabricate i-FLG electrodes and use them to produce functioning OPV devices, using PTB7/PC70BM Bulk Heterojunction (BHJ) active layer. The electrical conductivity, optical transmittance and surface morphology of i-FLG has already been characterized and published elsewhere (Khrapach et al., 2012; Bointon et al., 2014, 2015; Wehenkel et al., 2015; Walsh et al., 2018) by our group. These devices are compared to devices fabricated in tandem using commercially available ITO as the anode. While comparing device performance metrics is paramount to identifying new materials for OPV device fabrication, investigating the impact to device stability is also an important and often overlooked factor. As such, device stability studies under both continuous and periodic illumination were performed, the results give insight into methods of improving device stability by the replacement of ITO as the anode material.

2. MATERIALS AND METHODS

Here, we detail the materials and methods used in the fabrication and characterization of OPV devices made with ITO and i-FLG electrodes.

2.1. Fabrication

Transfer and intercalation of FLG samples was performed following the procedures set out in previous works (Khrapach et al., 2012; Walsh et al., 2018). FLG samples grown on $Ni/Si/SiO_2$ substrates were purchased from Graphene Supermarket, and coated with a protective layer of Poly(Methyl Methacrylate) (PMMA). A solution of $FeCl_3$ was used to etch the Ni catalyst, allowing the FLG to be transferred to a glass substrate. After cleaning and removal of the PMMA protective layer using washes in Acetone and Isopropyl Alcohol (IPA), FLG samples were intercalated with $FeCl_3$ using a three zone furnace method. The $FeCl_3$ intercalant was heated to a temperature of 315°C causing it to sublimate, while the sample was maintained at a temperature of 360°C. This allows the molecules of $FeCl_3$ to penetrate between the graphene layers, intercalating the FLG sample.

Before being used in OPV devices, i-FLG electrodes were cleaned using a 5 min UV/Ozone treatment (UV/Ozone Cleaner, Ossila) in order to improve the wetting of the i-FLG surface by the hole transport layer (HTL). OPV device fabrication was performed following the standard design and blend ratios for PTB7:PC70BM OPV devices (He et al., 2011; Ding et al., 2016). An aqueous solution of poly(3,4-ethylenedioxythiophene) polystyrene sulfonate (PEDOT:PSS), purchased from Ossila (HTL Solar, Ossila), is spin coated to form a 40 nm thick HTL over the i-FLG anode. The Bulk Heterojunction (BHJ) active

layer solution is prepared from a mixture of Poly[[4,8-bis[(2-ethylhexyl)oxy]benzo[1,2-b:4,5-b']dithiophene-2,6-diyl][3-fluoro-2-[(2-ethylhexyl)carbonyl]thieno[3,4-b]thiophenediyl]] (PTB7) polymer donor and Phenyl-C70-butyric acid methyl ester (PC70BM) fullerene acceptor. These two compounds are mixed in a 1.5:1 ratio in a solution of Dichlorobenzene (DCB) with 3%/vol 1,8-Diiodooctane (DIO). This BHJ solution is then spincoated onto the HTL for a thickness of 90 nm. Finally, a Zinc Oxide (ZnO) Electron Transport Layer (ETL) is spincoated onto the BHJ and an Aluminum cathode deposited by thermal evaporation, using a custom built evaporation mask to define the solar cell active area. Devices were not encapsulated such that the impact of atmospheric degradation on the devices could be understood.

2.2. Characterization

Raman Spectroscopy was used to characterize the i-FLG, as has been extensively demonstrated in previous works. A custom built multipurpose microscope was used (Sanctis et al., 2017), with a 30–50 mW, 514 nm laser (2 s exposure time, 1 μm spot diameter). Raman spectra were taken periodically over a 30 × 30 μm area, allowing a Raman map to be produced. The doping across the sample can be observed through the relative shift in the G peak position of the Raman spectrum. Hence, Raman maps could be used to characterize the average doping in the sample.

The sheet resistance of graphene samples was measured by the 4-point probe method after the samples had been intercalated. Work Function values for the samples were measured by Scanning Kelvin Prove Force Microscopy (SKPFM) over a 20 × 20 μm area.

A class ABB solar simulator (Newport, 94011A) is used to expose OPV devices to a AM1.5G spectrum with an irradiance of 1 Sun. Current-Voltage (IV) characteristics are measured, running forward and reverse voltage sweeps between 1 and −1 V, with a voltage step of 10 mV and a settle time of 10 ms. Measurements were taken in both light and dark conditions to fully characterize the devices. The stability of the OPV devices was investigated in two manners, one where the device performance was measured under continuous illumination and another where the devices were periodically characterized in between being stored in a desiccator. Four curves were taken every 60 s under continuous illumination over a period of 1 h, while under periodic illumination devices were characterized multiple times over the period of 11 days, or until the device failed.

3. RESULTS

Figure 1A shows an optical image of the intercalated graphene electrode on a quartz substrate. The inset shows a magnified optical microscope image of the FLG film (scale bar shown). Ni grown CVD graphene grows in a patchwork manner, with individual graphene domains spanning some 10's of μm. This gives the surface of the sample an inherent roughness due to the variation in number of layers in each graphene domain. This also produces variation in the doping of the intercalated sample, due to variation in the staging of the intercalant molecules. Raman spectroscopy is used to characterize the doping of the graphene sample, which gives access to a wide variety of important information such as the doping conditions, strain, and number of layers among others. The doping level can be easily extracted by calculating the relative shift in G-peak compared to an undoped sample as was described by Lazzeri and Mauri (2006). **Figure 1B** shows the G-peak of the Raman spectrum for an i-FLG sample. The G-peak is composed of three subpeaks, relating to different doping environments in the sample caused by the aforementioned variation in intercalant staging. This can be quantified by the relative G-peak shift metric, $\langle PosG \rangle$ (Walsh et al., 2018), as shown by Equation (1).

$$\langle PosG \rangle = \frac{PosG_0 \frac{AreaG_0}{2} + \sum_{i=1}^{2} PosG_i AreaG_i}{\frac{AreaG_0}{2} + \sum_{j=1}^{2} AreaG_j}, \quad (1)$$

This metric weighs the relative peak shift of each sub-peak by its area (half area for G0 peak, as the G-peak narrows with doping; Pisana et al., 2007; Das et al., 2008), normalized to the total area of the peak. Using this PosG metric, a map of the intercalation across a 30 × 30 μm area was generated in **Figure 1C**. The maps of various areas are then converted to histograms to better compare the degree of intercalation in different samples. In **Figure 1D**, we show the PosG histograms for pristine and intercalated samples, with the average PosG values displayed above their respective histograms. Variation in the value of ⟨PosG⟩ is caused by the variation in the sample thickness. This produces different staging conditions, as thicker areas of graphene typically intercalate better than thin areas, thereby receiving a higher level of doping. From the histogram it is clear to see that the entire sample has been intercalated, resulting in a highly doped electrode material with reduced sheet resistance and increased work function.

OPV devices with the structure Quartz/Anode/PEDOT:PSS/PTB7:PC70BM/ZnO/Al were fabricated, using both ITO and i-FLG as the anode materials, respectively. **Figure 2A** shows the structure for devices utilizing i-FLG as the anode. In this structure the absorption of photons occurs in the BHJ layer (PTB7:PC70BM), forming excitons which diffuse through the BHJ layer until they reach a boundary at the donor/acceptor interface (Yan et al., 2018). This allows the exciton to separate into charge carriers (electrons and holes), which are then transported through the donor/acceptor materials and electron/hole transport layers. The energy band structure that is produced as a result of device structure is shown in **Figure 2B**. The band gap of the solar cell is defined by the difference in the energy of the HOMO of the donor compound and the LUMO of the acceptor compound, which in this case is 1.1 eV. The key difference between the two devices fabricated lies in the differences between their electrodes. The i-FLG electrode possesses a much higher work function due to the lowered Fermi level of the graphene layers caused by p-doping from intercalation. The work function of i-FLG allows for a better match to the energy level of the hole transport layer (PEDOT:PSS). This leads to an improvement in charge extraction capabilities of the OPV device when

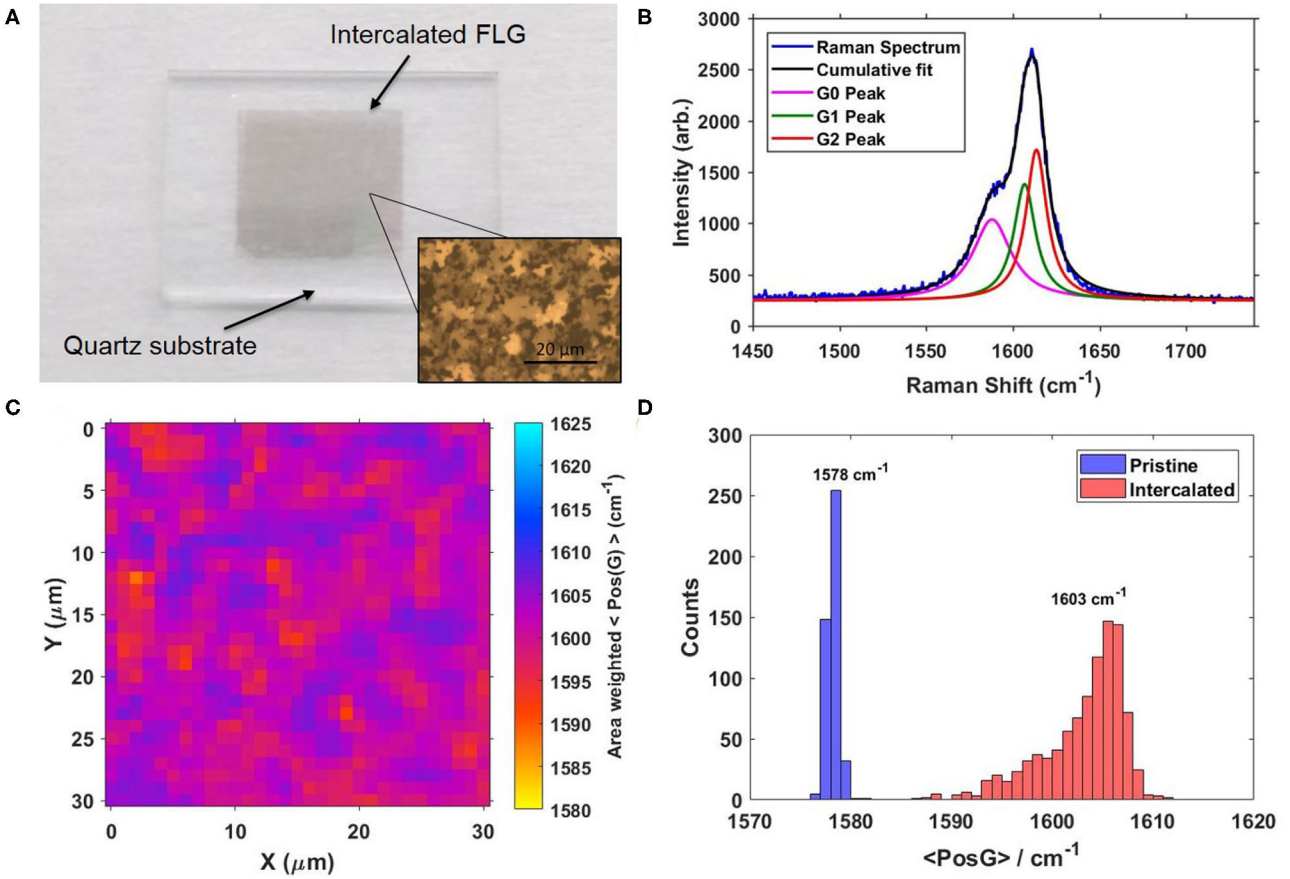

FIGURE 1 | (A) Image of 1 × 1 cm $FeCl_3$ intercalated Few Layer Graphene electrode with magnified insert showing patchwork structure of the Ni CVD graphene. **(B)** G-peak of the Raman spectrum of $FeCl_3$ intercalated graphene. p-doping causes a stiffening of the G-peak, forming three sub-peaks (G0, G1, and G2), each relating to a different staging of intercalant. **(C)** Raman map of intercalated graphene sample showing the in G peak as calculated by our ⟨ PosG ⟩ metric. Variation in ⟨ PosG ⟩ is caused by the non-uniformity of the few layer graphene thickness, with higher doping (and hence ⟨ PosG ⟩) in thicker areas of the sample. **(D)** Histogram constructed from 30 × 30 μm Raman maps of Pristine and i-FLG samples.

compared to ITO counterpart devices. Such improvement can be seen in **Figure 2C** from the shape of the i-FLG device's IV curve. The IV curve is used to assess the performance of the solar cell devices by comparing calculated efficiency values, along with many other device performance metrics. The increased work function of the i-FLG electrodes leads to an increased fill factor of 47.5% compared to 36.4% for ITO devices, as well as a lowered series resistance and increased shunt resistance. However, ITO devices performed better with a peak efficiency of 3.15% and an average device efficiency of 2.43 ± 0.11%, compared to a peak and average efficiency of 2.78% and 1.83 ± 0.29% for the i-FLG devices. Average device efficiencies were calculated from 11 ITO devices and 5 i-FLG devices. The higher efficiency is due to the larger J_{SC} for ITO devices caused by ITO's high transmittance of around 85%, compared to i-FLG's transmittance of 75% at 550 nm (**Supplementary Figure 1**). This allows for the absorption of a greater number of photons by the BHJ and therefore the generation of a larger photocurrent. Despite this, the difference in device efficiency is relatively small, while it can be seen that there is a significant improvement to charge transport when using the i-FLG electrodes.

After the basic characterization of the OPV devices, their stability to atmospheric degradation was investigated by measuring device performance under continuous illumination. The reduction in performance is a result of both the continued exposure to light and the damage caused to the devices from atmospheric factors, such as humidity and oxidation of active layers (Yilmaz et al., 2017). Device efficiencies displayed have been normalized to the device's performance at the beginning of measurement to better show the change in performance over time. **Figure 3A** shows the normalized efficiency data for both devices over the first hour of testing. As is clearly shown in the graph, the efficiency of the ITO device degrades much more rapidly than the i-FLG device, dropping by 20% of its original efficiency over the first 30 min before the rate of degradation begins to decrease. i-FLG devices show a far slower rate of degradation, exhibiting a linear drop in efficiency of around 5% over the full hour of exposure, compared to a drop of more than 25% observed for ITO devices. This

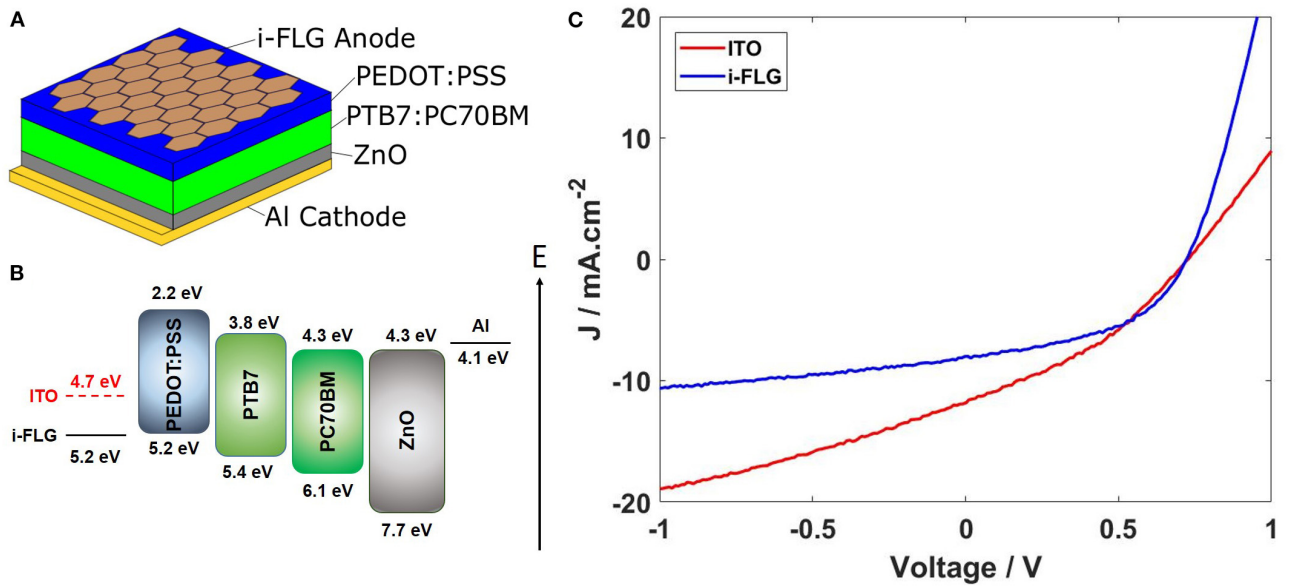

FIGURE 2 | (A) IV curves for the best performing OPV devices with ITO and i-FLG electrodes, respectively (Dark curves provided in **Supplementary Material**). **(B)** Energy level diagram for the OPV devices investigated. Work function of i-FLG electrode is as measured by SKPFM, while a literature reference was used for ITO. **(C)** OPV device diagram.

drop in efficiency is primarily caused by a drop in short circuit current observed for both devices. However, as with efficiency, the short circuit current for ITO devices drops far more rapidly than for i-FLG devices, as shown in **Figure 3B**. In addition to the drop in the short circuit current, it can be seen that the series resistance of the ITO devices also increases faster than i-FLG under the same illumination conditions (**Figure 3C**). The series resistance of i-FLG electrodes only increases very slightly over the course of the testing, remaining below 40 Ω cm^2 for the full duration of the investigation. ITO device series resistance, however, is around 60 Ω cm^2 at the start of the measurement and varies by as much as 20 Ω cm^2 between each measurement, eventually increasing by approximately 25 Ω cm^2 after the hour of testing. The shunt resistance for both sets of devices varied significantly during the continuous illumination measurements. However, the average values remained constant at around 140 Ωcm^{-2} for ITO and 115 Ωcm^{-2} for i-FLG devices (**Supplementary Figure 6**). The lower shunt resistance of i-FLG devices indicates alternate current paths present in the BHJ and are likely due to variation in OPV batches as opposed to originating from a difference in the electrodes. These results indicate that not only is i-FLG a better performing electrode in terms of charge extraction, but it is also much more resilient to the degradation associated with device operation.

The decay behavior shown by the ITO based devices is typical for many OPV devices, showing an initial rapid decrease in efficiency in what is known as the burn in phase, before reverting to a slower rate of degradation (Mateker and McGehee, 2017). Fitting both sets of data with decay equations we find that i-FLG devices' decay obeys a zeroth order decay law, while ITO devices obey a second order decay law; as described by Equations (2) and (3), respectively.

$$E(t) = E(0)\lambda t \tag{2}$$

$$\frac{1}{E_{(t)}} = -\lambda t + \frac{1}{E_0} \tag{3}$$

where E_0 is the efficiency at time $t = 0$, $E(t)$ is the efficiency measured after some time, t, and λ is the decay constant. The higher order decay rate exhibited by ITO devices is likely due to additional intrinsic/extrinsic factors affecting the device degradation in ITO devices, compared to i-FLG devices. This means that while both devices will be similarly impacted by the atmospheric conditions the devices are exposed to, additional factors are impacting the ITO devices. A prime contender for a key aspect of device degradation that impacts ITO based devices more strongly than i-FLG devices is the acidity of the PEDOT:PSS layer damaging the ITO electrode (Girtan and Rusu, 2010; Sharma et al., 2011). This explains the rise in series resistance of ITO devices and why i-FLG devices did not exhibit the same increase. In addition, this damage to the ITO can result in the ingress of indium ions into the polymer layers of the device, further accelerating device degradation by the creation of defects in the active layers of the device. Such a diffuse contact can cause the formation of large area charge blocking layers, this has also been observed to occur at the Al cathode due to the oxidation of the Al at the Al/ZnO interface (Wang et al., 2011). i-FLG has been shown to be very resilient to damage from a range of environmental conditions, such as corrosive environments (Srimaneepong et al., 2020) or high temperature and humidity (Wehenkel et al., 2015). It is likely that resistance to acidic

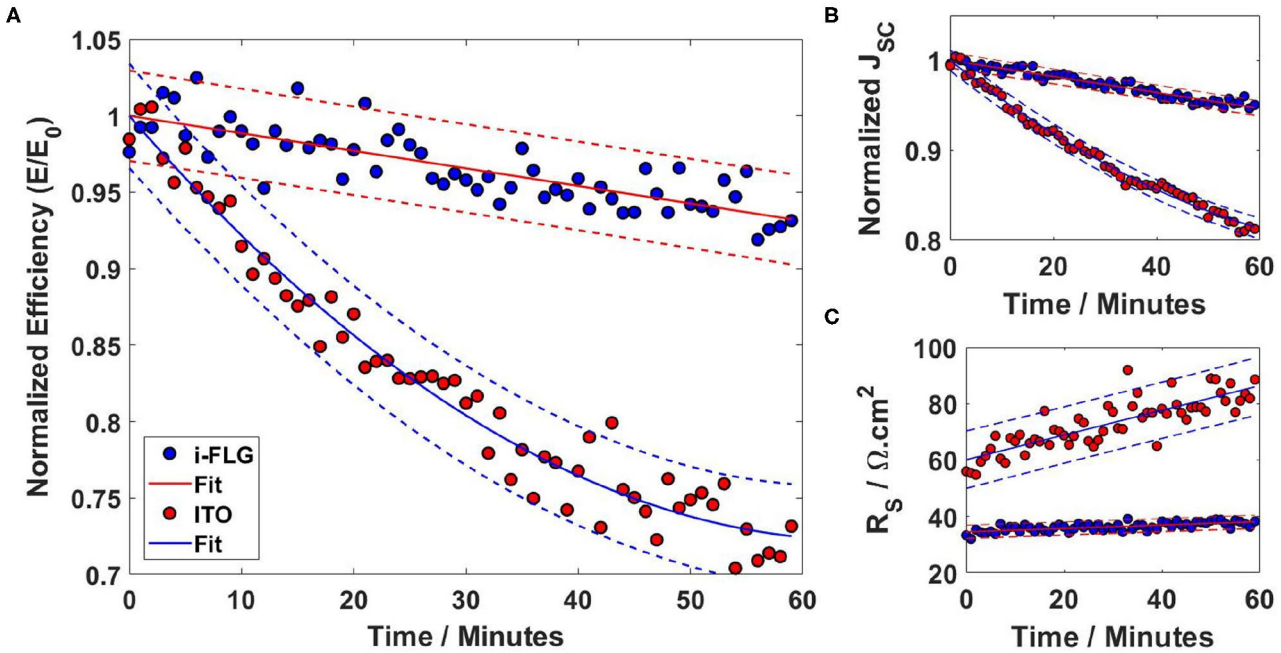

FIGURE 3 | (A) Normalized efficiency stability over time for ITO and i-FLG devices. Solid lines show the fit to the data, dashed lines show 95% confidence range. Data is normalized to the performance of the device at $t = 0$. **(B)** Variation in Normalized short circuit current over time. **(C)** Variation in device series resistance over time.

conditions prevents damage to the i-FLG electrode, while the ITO electrode is very susceptible to this type of damage, although this would require further study to explicitly demonstrate. Other sources of degradation that will still affect the i-FLG devices are primarily the ingress of water and air molecules into the device active layers. This causes the oxidation of the donor and acceptor molecules, increasing trap density and lowering the photocurrent generated by the cell.

Figure 4 shows the performance of the i-FLG and ITO based OPV devices subjected to periodic illumination. Under these conditions, devices performed for a much greater length of time before degrading, i.e., for more than 250 h as compared to devices subjected to continuous illumination. This effect may be due to the fact that the devices were stored in a desiccator between each successive measurement, limiting the damage to the device that could be caused by exposure to light and atmospheric factors such as humidity and exposure to oxygen. When comparing the performance of i-FLG devices with ITO devices (**Figure 4A**), we observed that after 3 days from the first measurement, both sets showed an increase in the normalized efficiency caused by an increase in the open circuit voltage of both devices (shown in **Figure 4B** for ITO and **Figure 4C** for i-FLG). This is likely due to the removal of remnant solvent in the BHJ during the period in the desiccator, allowing the donor/acceptor compounds to rearrange in the BHJ. Such an effect would reduce unwanted charge carrier recombination, increasing the open circuit voltage. What is most notable in this measurement is that after 100 h all ITO devices had failed, while all i-FLG devices maintained a better performance than their original measurement for more than 250 h. This indicates that i-FLG has the potential to greatly improve the lifetime of OPV devices, removing the unstable and costly ITO from the devices entirely.

4. DISCUSSION

In conclusion, our investigation raises evidence that the replacement of ITO electrodes in OPV devices can greatly improve the stability of the device's performance. $FeCl_3$ Intercalated FLG electrode based devices proved to be much more stable than ITO based devices under both continuous and periodic illumination. This highlights a relatively unexplored benefit of replacing ITO with graphene based transparent electrodes in OPV devices. The key aspect of device degradation that impacts ITO based devices more strongly than i-FLG devices is the acidity of the PEDOT:PSS layer damaging the ITO electrode. This effect leads to an increase in series resistance of ITO devices, while i-FLG devices did not exhibit the same effect. Indeed, i-FLG has been shown to be very resilient to damage from many sources, but most notably from high pH acids, such as HCl, due to the impressive chemical inertness of the graphene surface (Singh Raman and Tiwari, 2014; Kwon et al., 2018). In the absence of degradation due to acidity, device performance is primarily effected by the ingress of water and air molecules into the device active layers. Device efficiencies were lower than similar OPV devices published in the literature for both ITO and i-FLG electrodes. This is likely caused by the commercially available materials used in the BHJ, and the fabrication of the OPV devices not yet being fully optimized. As higher efficiencies have been demonstrated for ITO devices in the past, it is

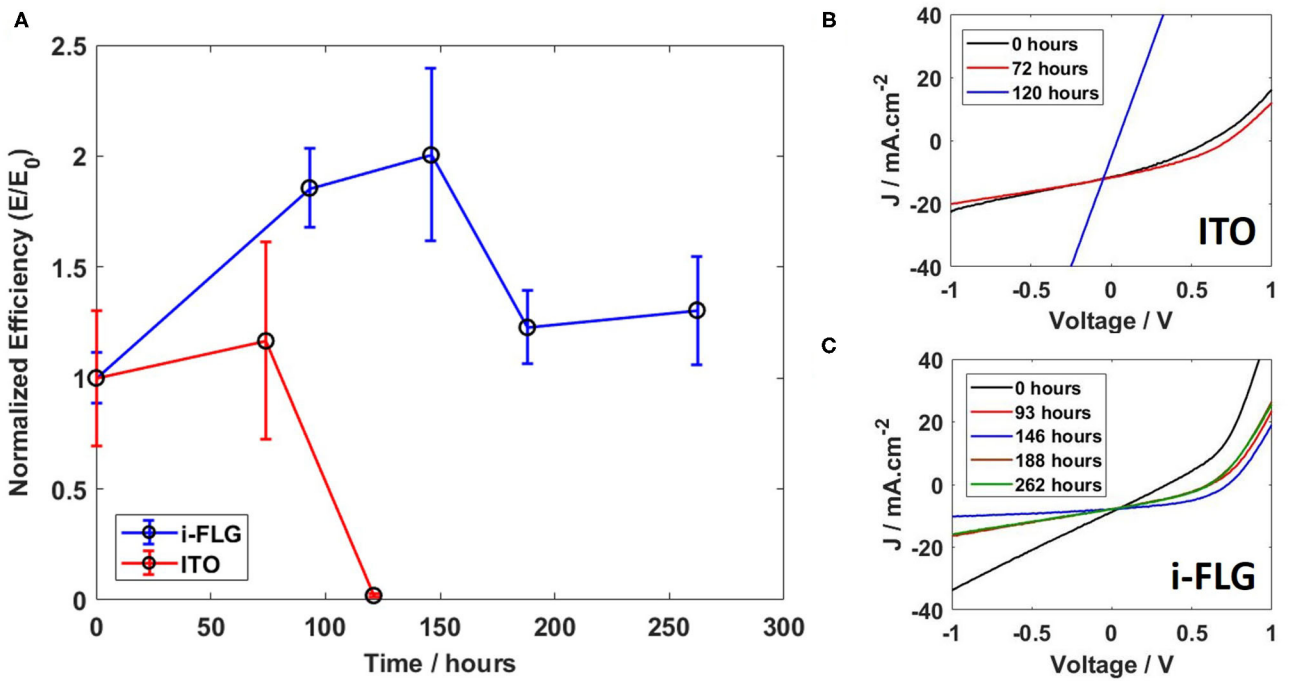

FIGURE 4 | (A) Normalized periodic stability for devices intermittently stored in a desiccator. **(B,C)** IV curves for periodic efficiency measurements for ITO **(B)** and i-FLG **(C)** devices.

likely that even higher efficiencies can also be achieved for i-FLG devices also. Once fully optimized, future work should focus on investigating the i-FLG device flexibility and changes in performance. Previous investigations have highlighted that graphene based electrodes outperform ITO devices under bent conditions (Kymakis et al., 2013). It is also highly probable that device stability and lifetimes could be improved by using device encapsulation procedures.

DATA AVAILABILITY STATEMENT

The research data supporting this publication are openly available from the University of Exeter's institutional repository at: https://doi.org/10.24378/exe.2984.

AUTHOR CONTRIBUTIONS

All OPV devices were fabricated and characterized by KW. KW and CM contributed to the transfer, intercalation, and characterization of intercalated graphene electrodes. Project motivation and guidance were provided by MC and SR. All authors contributed to the article and approved the submitted version.

FUNDING

The authors acknowledge financial support from the UK Engineering and Physical Sciences Research Council (EPSRC) via the centre for doctoral training in metamaterials at University of Exeter and (Grant Nos. EP/K010050/1, EP/M001024/1, and EP/M002438/1) and the Leverhulme Trust (Grant Quantum Revolution).

SUPPLEMENTARY MATERIAL

The Supplementary Material for this article can be found online at: https://www.frontiersin.org/articles/10.3389/felec.2021.643687/full#supplementary-material

REFERENCES

Balis, N., Stratakis, E., and Kymakis, E. (2016). Graphene and transition metal dichalcogenide nanosheets as charge transport layers for solution processed solar cells. *Mater. Today* 19, 580–594. doi: 10.1016/j.mattod.2016.03.018

Bhandari, K. P., Collier, J. M., Ellingson, R. J., and Apul, D. S. (2015). Energy payback time (EPBT) and energy return on energy invested (EROI) of solar photovoltaic systems: a systematic review and meta-analysis. *Renew. Sustain. Energy Rev.* 47, 133–141. doi: 10.1016/j.rser.2015.02.057

Bointon, T. H., Jones, G. F., De Sanctis, A., Hill-Pearce, R., Craciun, M. F., and Russo, S. (2015). Large-area functionalized CVD graphene for work function matched transparent electrodes. *Sci. Rep.* 5:16464. doi: 10.1038/srep16464

Bointon, T. H., Khrapach, I., Yakimova, R., Shytov, A. V., Craciun, M. F., and Russo, S. (2014). Approaching magnetic ordering in graphene materials by FeCl3 intercalation. *Nano Lett.* 14, 1751–1755. doi: 10.1021/nl4040779

Brunetti, F., Ulisse, G., Dianetti, M., Susanna, G., Innaccone, G., Fiori, G., et al. (2015). "Doped and textured graphene as electrode for organic solar cells," in *Proceedings for the 2015 IEEE 15th International Conference on Nanotechnology (IEEE-NANO)* (Rome), 560–563. doi: 10.1109/NANO.2015.7388666

Castro Neto, A. H., Guinea, F., Peres, N. M. R., Novoselov, K. S., and Geim, A. K. (2009). The electronic properties of graphene. *Rev. Modern Phys*. 81, 109–162. doi: 10.1103/RevModPhys.81.109

Darling, S. B., and You, F. (2013). The case for organic photovoltaics. *RSC Adv*. 3, 17633–17648. doi: 10.1039/c3ra42989j

Das, A., Pisana, S., Chakraborty, B., Piscanec, S., Saha, S. K., Waghmare, U. V., et al. (2008). Monitoring dopants by Raman scattering in an electrochemically top-gated graphene transistor. *Nat. Nanotechnol*. 3, 210–215. doi: 10.1038/nnano.2008.67

de Sanctis, A., Jones, G. F., Wehenkel, D. J., Bezares, F., Koppens, F. H., Craciun, M. F., et al. (2017). Extraordinary linear dynamic range in laser-defined functionalized graphene photodetectors. *arXiv*. doi: 10.1126/sciadv.1602617

Ding, Z., Kettle, J., Horie, M., Chang, S. W., Smith, G. C., Shames, A. I., et al. (2016). Efficient solar cells are more stable: the impact of polymer molecular weight on performance of organic photovoltaics. *J. Mater. Chem. A* 4, 7274–7280. doi: 10.1039/C6TA00721J

Espinosa, N., García-Valverde, R., Urbina, A., and Krebs, F. C. (2011). A life cycle analysis of polymer solar cell modules prepared using roll-to-roll methods under ambient conditions. *Solar Energy Mater. Solar Cells* 95, 1293–1302. doi: 10.1016/j.solmat.2010.08.020

Espinosa, N., Hösel, M., Angmo, D., and Krebs, F. C. (2012). Solar cells with one-day energy payback for the factories of the future. *Energy Environ. Sci*. 5, 5117–5132. doi: 10.1039/C1EE02728J

Fthenakis, V. M., and Kim, H. C. (2011). Photovoltaics: life-cycle analyses. *Solar Energy* 85, 1609–1628. doi: 10.1016/j.solener.2009.10.002

Gallardo, D. E., Bertoni, C., Dunn, S., Gaponik, N., and Eychmüller, A. (2007). Cathodic and anodic material diffusion in polymer/semiconductor-nanocrystal composite devices. *Adv. Mater*. 19, 3364–3367. doi: 10.1002/adma.200700394

Girtan, M., and Rusu, M. (2010). Role of ITO and PEDOT:PSS in stability/degradation of polymer:fullerene bulk heterojunctions solar cells. *Solar Energy Mater. Solar Cells* 94, 446–450. doi: 10.1016/j.solmat.2009.10.026

Glen, T. S., Scarratt, N. W., Yi, H., Iraqi, A., Wang, T., Kingsley, J., et al. (2016). Dependence on material choice of degradation of organic solar cells following exposure to humid air. *J. Pol. Sci. Part B* 54, 216–224. doi: 10.1002/polb.23905

He, Z., Zhong, C., Huang, X., Wong, W. Y., Wu, H., Chen, L., et al. (2011). Simultaneous enhancement of open-circuit voltage, short-circuit current density, and fill factor in polymer solar cells. *Adv. Mater*. 23, 4636–4643. doi: 10.1002/adma.201103006

Khrapach, I., Withers, F., Bointon, T. H., Polyushkin, D. K., Barnes, W. L., Russo, S., et al. (2012). Novel highly conductive and transparent graphene-based conductors. *Adv. Mater*. 24, 2844–2849. doi: 10.1002/adma.201200489

Kwon, S. J., Han, T. H., Ko, T. Y., Li, N., Kim, Y., Kim, D. J., et al. (2018). Extremely stable graphene electrodes doped with macromolecular acid. *Nat. Commun*. 9, 1–9. doi: 10.1038/s41467-018-04385-4

Kymakis, E., Savva, K., Stylianakis, M. M., Fotakis, C., and Stratakis, E. (2013). Flexible organic photovoltaic cells with in situ nonthermal photoreduction of spin-coated graphene oxide electrodes. *Adv. Funct. Mater*. 23, 2742–2749. doi: 10.1002/adfm.201202713

Kymakis, E., Stratakis, E., Stylianakis, M. M., Koudoumas, E., and Fotakis, C. (2011). Spin coated graphene films as the transparent electrode in organic photovoltaic devices. *Thin Solid Films* 520, 1238–1241. doi: 10.1016/j.tsf.2011.04.208

Lazzeri, M., and Mauri, F. (2006). Nonadiabatic Kohn anomaly in a doped graphene monolayer. *Phys. Rev. Lett*. 97, 29–32. doi: 10.1103/PhysRevLett.97.266407

Lee, C., Wei, X., Kysar, J. W., and Hone, J. (2008). Measurement of the elastic properties and intrinsic strength of monolayer graphene. *Science* 321, 385–388. doi: 10.1126/science.1157996

Malinowski, M., Leon, J. I., and Abu-Rub, H. (2017). Solar photovoltaic and thermal energy systems: current technology and future trends. *Proc. IEEE* 105, 2132–2146. doi: 10.1109/JPROC.2017.2690343

Mateker, W. R., and McGehee, M. D. (2017). Progress in understanding degradation mechanisms and improving stability in organic photovoltaics. *Adv. Mater*. 29. doi: 10.1002/adma.201603940

Nair, R. R., Blake, P., Grigorenko, A. N., Novoselov, K. S., Booth, T. J., Stauber, T., et al. (2008). Fine structure constant defines visual transparency of graphene. *Science* 320, 1308–1308. doi: 10.1126/science.1156965

Novoselov, K. S., Geim, A. K., Morozov, S. V., Jiang, D., Zhang, Y., Dubonos, S. V., et al. (2004). Electric field effect in atomically thin carbon films. *Science* 306, 666–669. doi: 10.1126/science.1102896

Novoselov, K. S., Jiang, D., Schedin, F., Booth, T. J., Khotkevich, V. V., Morozov, S. V., et al. (2005). Two-dimensional atomic crystals. *Proc. Natl. Acad. Sci. U.S.A*. 102, 10451–10453. doi: 10.1073/pnas.0502848102

Pehl, M., Arvesen, A., Humpenöder, F., Popp, A., Hertwich, E. G., and Luderer, G. (2017). Understanding future emissions from low-carbon power systems by integration of life-cycle assessment and integrated energy modelling. *Nat. Energy* 2, 939–945. doi: 10.1038/s41560-017-0032-9

Pisana, S., Lazzeri, M., Casiraghi, C., Novoselov, K. S., Geim, A. K., Ferrari, A. C., et al. (2007). Breakdown of the adiabatic Born-Oppenheimer approximation in graphene. *Nat. Mater*. 6, 198–201. doi: 10.1038/nmat1846

Razzell-Hollis, J., Wade, J., Tsoi, W. C., Soon, Y., Durrant, J., and Kim, J. S. (2014). Photochemical stability of high efficiency PTB7:PC70BM solar cell blends. *J. Mater. Chem. A* 2, 20189–20195. doi: 10.1039/C4TA05641H

Sanctis, A. D., Jones, G. F., Townsend, N. J., Craciun, M. F., and Russo, S. (2017). Thin optoelectronic devices: an integrated and multi-purpose microscope for the characterization of atomically thin optoelectronic devices. *Rev. Sci. Instrum*. 88. doi: 10.1063/1.4982358

Sharma, A., Andersson, G., and Lewis, D. A. (2011). Role of humidity on indium and tin migration in organic photovoltaic devices. *Phys. Chem. Chem. Phys*. 13, 4381–4387. doi: 10.1039/c0cp02203a

Shin, D. H., Jang, C. W., Lee, H. S., Seo, S. W., and Choi, S. H. (2018). Semitransparent flexible organic solar cells employing doped-graphene layers as anode and cathode electrodes. *ACS Appl. Mater. Interfaces* 10, 3596–3601. doi: 10.1021/acsami.7b16730

Singh Raman, R. K., and Tiwari, A. (2014). Graphene: The thinnest known coating for corrosion protection. *Jom* 66, 637–642. doi: 10.1007/s11837-014-0921-3

Speller, E. M., Clarke, A. J., Aristidou, N., Wyatt, M. F., Francás, L., Fish, G., et al. (2019). Toward improved environmental stability of polymer: Fullerene and polymer: Nonfullerene organic solar cells: a common energetic origin of light- and oxygen-induced degradation. *ACS Energy Lett*. 4, 846–852. doi: 10.1021/acsenergylett.9b00109

Srimaneepong, V., Rokaya, D., Thunyakitpisal, P., Qin, J., and Saengkiettiyut, K. (2020). Corrosion resistance of graphene oxide/silver coatings on Ni-Ti alloy and expression of IL-6 and IL-8 in human oral fibroblasts. *Sci. Rep*. 10, 1–12. doi: 10.1038/s41598-020-60070-x

Sun, T., Wang, Z. L., Shi, Z. J., Ran, G. Z., Xu, W. J., Wang, Z. Y., et al. (2010). Multilayered graphene used as anode of organic light emitting devices. *Appl. Phys. Lett*. 96, 4–7. doi: 10.1063/1.3373855

Torres Alonso, E., Karkera, G., Jones, G. F., Craciun, M. F., and Russo, S. (2016). Homogeneously bright, flexible, and foldable lighting devices with functionalized graphene electrodes. *ACS Appl. Mater. Interfaces* 8, 16541–16545. doi: 10.1021/acsami.6b04042

Walsh, K., Jones, G., Barnes, M., Murphy, C., De Sanctis, A., Russo, S., et al. (2018). Wafer scale FeCl3 intercalated graphene electrodes for photovoltaic applications. *Photon. Solar Energy Syst. VII* 10688:52. doi: 10.1117/12.2307410

Wang, M., Xie, F., Du, J., Tang, Q., Zheng, S., Miao, Q., et al. (2011). Degradation mechanism of organic solar cells with aluminum cathode. *Solar Energy Mater. Solar Cells* 95, 3303–3310. doi: 10.1016/j.solmat.2011.07.020

Wehenkel, D. J., Bointon, T. H., Craciun, M. F., Russo, S., Sciences, P., and Engineering, N. (2015). Unforeseen high temperature and humidity stability of FeCl 3 intercalated few layer graphene. *Sci. Rep*. 5:7609. doi: 10.1038/srep07609

Weu, A., Kress, J. A., Paulus, F., Becker-Koch, D., Lami, V., Bakulin, A. A., et al. (2019). Oxygen-induced doping as a degradation mechanism in highly efficient organic solar cells. *ACS Appl. Energy Mater*. 2, 1943–1950. doi: 10.1021/acsaem.8b02049

Withers, F., Bointon, T. H., Craciun, M. F., and Russo, S. (2013). All-graphene photodetectors. *ACS Nano* 7, 5052–5057. doi: 10.1021/nn4005704

Wong, H. C., Li, Z., Tan, C. H., Zhong, H., Huang, Z., Bronstein, H., et al. (2014). Morphological stability and performance of polymer-fullerene solar cells under thermal stress: the impact of photoinduced PC60BM oligomerization. *ACS Nano* 8, 1297–1308. doi: 10.1021/nn404687s

Wu, X., Xu, H., Wang, Y., Rogach, A. L., Shen, Y., and Zhao, N. (2007). General observation of the memory effect in metal-insulator-ITO structures due to indium diffusion. *Adv. Mater.* 19, 3364–3367. doi: 10.1088/0268-1242/30/7/074002

Yan, C., Barlow, S., Wang, Z., Yan, H., Jen, A. K., Marder, S. R., et al. (2018). Non-fullerene acceptors for organic solar cells. *Nat. Rev. Mater.* 3, 1–19. doi: 10.1038/natrevmats.2018.3

Yilmaz, E. e., Yeşilyurt, M. K., Öner, I. V., Ömeroğlu, G., and Özakin, A. N. (2017). Operational stability and degradation of organic solar cells. *Period. Eng. Nat. Sci.* 5, 152–160. doi: 10.21533/pen.v5i2.105

Conflict of Interest: The authors declare that the research was conducted in the absence of any commercial or financial relationships that could be construed as a potential conflict of interest.